HHS Public Access

Author manuscript

Mol Imaging. Author manuscript; available in PMC 2015 July 07.

Published in final edited form as:

Mol Imaging. 2013 September ; 12(6): 357–363.

In Vivo Demonstration of Cancer Molecular Imaging with Ultrasound Radiation Force and Buried-Ligand Microbubbles

Mark A. Borden[a,*], **Jason E. Streeter**[b], **Shashank R. Sirsi**[a], and **Paul A. Dayton**[b]

[a]Department of Mechanical Engineering, University of Colorado, Boulder, CO 80302

[b]Joint Department of Biomedical Engineering, University of North Carolina Chapel Hill and North Carolina State University, Chapel Hill, NC 27599

Abstract

In designing targeted contrast agent materials for imaging, the need to present a targeting ligand for recognition and binding by the target is counterbalanced by the need to minimize interactions with plasma components and to avoid recognition by the immune system. We have previously reported on a microbubble imaging probe for ultrasound molecular imaging that uses a buried-ligand surface architecture to minimize unwanted interactions and immunogenicity. Here we examine for the first time the utility of this approach for in vivo molecular imaging. In accordance with previous results, we showed a threefold increase in circulation persistence through the tumor of a fibrosarcoma model in comparison with controls. The buried-ligand microbubbles were then activated for targeted adhesion through the application of noninvasive ultrasound radiation forces applied specifically to the tumor region. Using a clinical ultrasound scanner, microbubbles were activated, imaged, and silenced. The results showed visually conspicuous images of tumor neovasculature and a twofold increase in ultrasound radiation force enhancement of acoustic contrast intensity for buried-ligand microbubbles, whereas no such increase was found for exposed-ligand microbubbles. We therefore conclude that the use of acoustically active buried-ligand microbubbles for ultrasound molecular imaging bridges the demand for low immunogenicity with the necessity of maintaining targeting efficacy and imaging conspicuity in vivo.

Introduction

When multiple treatment options exist for the long-term care of the patient, improve diagnosis of tumor physiology and measures of response to therapy and disease progression can provide the detailed information necessary to select the most appropriate therapy.[1, 2] Imaging-based biomarkers are attractive as they provide physiologic information registered to anatomy. An example of an imaging biomarker in widespread use today is positron emission tomography (PET) of ^{18}F- fluorodeoxyglucose (FDG) to assess tumor cell metabolism, which can be registered to anatomy through either x-ray computed tomography (CT) or magnetic resonance imaging (MRI). The clinical impact of FDG-PET has led

*Corresponding Author: Mark Borden, Department of Mechanical Engineering, University of Colorado, 1111 Engineering Drive, Boulder, CO 80302, mark.borden@colorado.edu.

Financial disclosure of the reviewers: None reported.

clinicians to seek other imaging biomarkers, with an emphasis on the need to assess the growth of new blood vessels within the tumor and its periphery. Currently, no clinically approved imaging biomarker for tumor angiogenesis is available for widespread clinical application.

The advent of compact, portable, and inexpensive ultrasound scanners has led to their broad dissemination throughout the health care system, including tertiary care facilities. However, there is no mechanism by which unenhanced ultrasonography can detect molecular changes, such as the expression of vascular biomarkers. To address this need, injectable ultrasound molecular imaging probes based on acoustically responsive microbubbles have been developed to extract information about the microvasculature. Microbubbles are excellent intravascular contrast agents for ultrasound imaging owing to their high compressibility and resonant properties within the clinical ultrasound frequency band, allowing single-microbubble detection with a clinical imaging system.[3] Targeting ligands can be attached to the microbubble surface for molecular imaging. However, this architecture presents the hazard of nonspecific interactions with plasma components that may lead to nonspecific adhesion.

One additional concern for clinical application of exposed-ligand microbubbles is complement activation, which may affect the targeting specificity of the ligand, stimulate an undesired immune response, change the underlying physiology, and, in more severe cases, result in complement activation–related pseudoallergy (CARPA).[4] It is therefore necessary to avoid complement fixation and activation by the targeting ligand on the microbubble surface.

To address the problems of immunogenicity and specificity in ultrasound molecular imaging, we engineered microbubbles with a buried-ligand architecture (BLA) in which a hydrated polyethylene glycol (PEG) brush on the microbubble surface consists of two tiers: the ligand is attached to a short PEG tether surrounded by longer PEG chains that forms an overbrush (Figure 1A).[5, 6] The brush self-assembles as the underlying lipids adsorb and condense into a monomolecular encapsulation during microbubble fabrication. Shielding of the ligand by the methoxy-terminated PEG overbrush was shown to inhibit complement activation and increase circulation persistence in non–tumor-bearing rodents.[5, 7–9]

The molecular probe is designed for activation by ultrasound radiation force (USRF), a phenomenon in which momentum is transmitted from the acoustic wave to the microbubble and is amplified near microbubble resonance.[5, 7] High-speed videomicroscopy studies showed that the microbubble dynamics during USRF involves both axial displacement and volumetric oscilla- tions (Figure 1B).[10–12] This combination of a normal force pressing the microbubble against the endothelium and lateral surface dilatation and contraction allows the ligand and receptor molecules to penetrate the overbrush for binding. In previous in vitro studies, we found that microbubbles with the BLA can be targeted to cells with the application of USRF.[7] However, previous studies have not demonstrated in vivo ultrasound molecular imaging with buried-ligand microbubbles.

To test the functionality of the BLA, we elected to target the vasculature with the cyclo Arg-Gly-Asp (cRGD) peptide, which has been shown to target tumor vasculature through binding to $\alpha_v\beta_3$ integrin that is overexpressed in tumor vasculature.[13] Although cRGD may also bind to other integrins of the β3 family, such as platelet integrin $\alpha_{IIb}\beta_3$, the specific activation of the buried-ligand micro- bubbles through acoustic radiation force of tumor tissues is expected to limit nonspecific background. We adapted a clinical ultrasound scanner to provide three-dimensional B-mode images of anatomy, contrast-enhanced images of microbubble distribution, USRF pulses to mediate targeted adhesion, and higher intensity pulses to fragment micro- bubbles and thereby silence their signal. Comparison of in vivo results from exposed-ligand and buried-ligand microbubbles allowed an assessment of this approach for molecular imaging.

Materials and Methods

Microbubble Formulation

Peptide-labeled lipid microbubbles with BLA and exposed- ligand architecture (ELA) were prepared as described previously.[6, 8, 9] Briefly, a 2.0 mg/mL lipid suspension containing 90 mol% distearoylphosphatidylcholine (DSPC), 5 mol% dipalmitoyl phosphatidylethanolamine (DSPE)-PEG5000 (for BLA) or 5 mol% DSPE-PEG2000 (for ELA), and 5 mol% DSPE-PEG2000 maleimide (Avanti Polar Lipids, Alabaster, AL) was made in phosphate-buffered saline (PBS; pH 7.4). The ELA involves a tether length equal to the surrounding brush-forming polymers, and transient excursions of the tether provide exposure of the ligand to the milieu.[14] One hundred milliliters of the lipid solution was heated to 60°C and dispersed using a probe sonicator (Model 450A, Branson Ultrasonics, Danbury, CT). Microbubbles were formed by high-intensity probe sonication with a perfluorobutane (PFB) gas (FluoroMed, Round Rock, TX) atmosphere over the solution. Microbubbles were then washed and size selected to 4 to 5 μm diameter by centrifugation[15] and then resuspended in PBS (pH 6.5, 150 mM NaCl, 5 mM ethylenediaminetetraacetic acid [EDTA]) for conjugation with cysteine-labeled peptides.

Peptide Conjugation to Microbubbles

Microbubbles were labeled with cysteine-modified cRGD or cyclo Arg-Ala-Asp (cRAD) peptides (Peptides International; Louisville, KY), as previously described.[16] Peptides were dissolved in a degassed 3% acetic acid solution (10 mg/mL; Sigma Aldrich, St. Louis, MO) and combined with 1 mL of suspension containing maleimide-bearing micro- bubbles (1–5×10^9 MB/mL). The peptides were mixed with microbubbles at a 30:1 peptide to maleimide molar ratio to ensure complete binding of available maleimide groups. The peptides were conjugated to the microbubbles with gentle mixing (end over end) at 4uC overnight to allow the thiol- reactive maleimide groups on the microbubble surface to bind with the cysteine end-groups of the peptides. After incubation, the peptide-bearing microbubbles were washed to remove excess unconjugated peptides and concentrated by centrifugation. We previously showed that this metho- dology leads to a high coupling yield of RGD peptide to BLA microbubbles.[6, 8, 9, 17] Microbubbles were then resuspended in sterile PBS (pH 7.4, 150 mM NaCl) to a concentration of 5 to 8×10^8 MB/mL in 3 mL serum vials and then capped and sealed with a PFB headspace. All microbubbles were fabricated in Boulder, Colorado

(elevation 5,300 ft), and shipped to Chapel Hill, North Carolina (elevation 460 ft), where they were used without further modification for subsequent animal studies. The size distribution and concentration of microbubbles was measured at both locations using Accusizer 270A particle sizing instruments (Particle Sizing Systems, Santa Barbara, CA); the shipping and handling process resulted in no measurable change in microbubble size distribution or concentration. The microbubble samples were identified by their surface architecture (ELA vs BLA) and peptide ligand (cRGD vs cRAD).

Animals and Tumor Models

Eight Fischer 344 rats (Charles River Laboratories, Durham, NC) of similar size (≈250 g) were used for all imaging studies. The wild-type rats had an intact complement system.[18] Each animal study was conducted in accordance with the protocols approved by the Institutional Animal Care and Use Committee at the University of North Carolina School of Medicine. The tumor model used was the HT1080 fibrosarcoma, which has been shown to express $\alpha_v\beta_3$ integrin in nascent vasculature.[19, 20] Imaging was performed once the tumor had grown to approximately 1 cm in diameter in the longest measurable axis.

Animal Preparation and Contrast Administration

Animals were prepared for imaging by anesthetization with 2% inhaled isoflurane mixed with oxygen. Once sedated, the imaging area was shaved and depilated using a chemical hair remover. A 24-gauge catheter was inserted into the tail vein for the purpose of administering microbubbles into the circulatory system of the animal. For each injection, a dose of 5.0×10^6 microbubbles was administered and flushed with 100 mL of sterile saline. Animals received less than 1.5 mL of total fluid volume through the tail vein within any 24-hour period.

Four different types of microbubbles (ELA-cRGD, ELA-cRAD, BLA-cRGD, and BLA-cRAD) were evaluated with or without the application of USRF. Because of the dose limitations with the injected volume of saline into the animals, the imaging studies were performed over several days with multiple injections per animal. Each animal underwent no fewer than three bolus injections and no more than eight injections in one session. In addition, all bolus injections during an imaging session were administered to the animal in random order. If USRF was applied to a particular microbubble type in an imaging session, then molecular imaging with no USRF was also performed with the same microbubble type in the same imaging session. Between each bolus injection in a particular imaging session, there was a minimum wait time of 10 minutes to ensure that no circulating microbubbles remained in the tumor vasculature from the previous injection.

Clinical Imaging System

A clinical ultrasound system (Sequoia 512, Acuson, Mountain View, CA) was used to acquire all images in this study. B-mode images were collected at 14 MHz using a 15L8 linear array transducer in spatial compounding mode as a means for selecting the regions of interest (ROI) in each image plane. Microbubbles were imaged in cadence pulse sequencing (CPS) mode, which is a nondestructive contrast-specific imaging technique[21] available on commercial scanners. For all contrast imaging, the transducer was operating at a frequency

of 7 MHz, a mechanical index of 0.18, and a CPS gain of -12 dB. To create volumetric data sets, the ultrasound transducer was stepped elevationally using a motion stage (Model UTS150PP, Newport Corporation, Irvine, CA).[22] All images were saved in Digital Imaging and Communications in Medicine (DICOM) file format.

USRF pulses were created using the pulsed-wave Doppler mode at a center frequency of 7 MHz, a gate size of 18 mm, and a blood velocity scale of 1 m/s. These parameters enabled us to achieve a 25% duty cycle pulse with a pulse repetition frequency of 25 kHz. All USRF pulses used in this study were delivered at an output power value of -3 dB, which corresponds to a peak negative pressure amplitude of 13 kPa.[23] Volumetric applications of USRF were applied by stepping the ultrasound transducer elevationally using the motion stage.

Image Analysis

The saved DICOM images were analyzed and registered offline using custom MATLAB (Mathworks, Natick, MA) scripts and functions. Average video intensity (AVI) in units of decibels was obtained by summing the CPS video intensity values for each voxel within the ROI volume and dividing that value by the total number of voxels within that volume. The average contrast intensity (ACI) in units of decibels was computed by subtracting the background AVI obtained prior to the targeted micro- bubble injection from the AVI produced by the molecular imaging scan. This method of analysis provided a direct comparison between the different imaging parameters but did not correct for nonlinearities inherent in the imaging system.

Contrast Agent Persistence

Microbubble clearance from the circulatory system was determined by measuring the length of time that microbubbles persisted in the tumor vasculature. Only animal studies with contrast administration not requiring USRF were used to collect persistence data. Prior to obtaining molecular imaging data, circulation persistence times in the tumor were obtained at the cross-sectional center of the tumor. After each bolus injection, CPS images were recorded at a 1 Hz sample rate. Once no microbubbles were visibly moving in the vasculature, image acquisition was stopped and the CPS images were analyzed offline. Circulation half-life in units of seconds was calculated by taking the time from the peak ACI to the time that the ACI reached half of the peak value.[24]

Molecular Imaging

Once the circulating microbubbles had cleared, one CPS image frame was collected at every 400 μm as the transducer was stepped elevationally across the tumor. Next, the imaging system was set to a microbubble- silencing, B-mode setting with a center frequency of 7 MHz and a mechanical index of 1.9. Subsequently, the transducer was swept at 1 mm/s elevationally across the tumor to silence any adherent microbubbles remaining in the vasculature. The system was again set to image in CPS mode, and the tumor was reimaged at each location across the tumor to collect background image intensity data. To compare the molecular imaging data across animals, data were normalized to the ACI produced by the BLA-cRAD injection because this microbubble type was used in every animal. The

ultrasound contrast to tissue ratio in units of decibels for molecular imaging of $\alpha_v\beta_3$ integrin expression in the tumor (CTRmi) was determined by taking the difference in volumetric ACI before and after microbubble silencing. The dimensionless USRF enhancement of targeted adhesion for a given microbubble type was determined by taking the ratio of CTRmi with USRF to that without USRF. Previous work has shown that multiple injections of targeted micro- bubbles do not block sufficient binding sites to bias molecular imaging data in serial studies.[25] Additionally, previous analysis of biomarkers of renal injury and renal histopathology indicated that there was no significant renal damage due to these ultrasound parameters in conjunction with microbubbles.[26]

Statistical Analysis

All statistical analysis was performed using GraphPad Prism 5 (San Diego, CA) software. Comparisons of USRF enhancement between ELA-cRGD and BLA-cRGD were performed using the nonparametric, two-tailed Mann- Whitney test, and statistical significance for a difference between the median values was determined by $p<0.05$.

Results

Microbubble Circulation Persistence

We first investigated whether burying cRGD by the PEG overbrush can increase the circulation persistence of the microbubbles in tumor-bearing rats with an intact complement system. The microbubbles were isolated from lipid fragments and selected to 4 to 5 μm diameter using differential centrifugation.[15] The small molecule ligand was attached to the shorter PEG chain following microbubble fabrication and size selection.[6] Targeted microbubbles were injected into the tail vein of wild-type rats with HT1080 fibrosarcoma tumors implanted in the hindlimb.[19, 20] The persistence of ultrasound contrast enhancement was measured as a function of time in the tumor midsection for BLA-cRGD microbubbles, and the results were compared to those for microbubbles carrying ELA-cRGD (ie, not buried by PEG). We observed that the ultrasound contrast half-life in the tumor was over threefold higher for the buried-ligand microbubbles (Figure 2). The microbubbles were of similar size and concentration; therefore, the increase in circulation persistence indicated a functional decrease in nonspecific interactions between the ligand and mononuclear phagocyte system.

Ultrasound Molecular Imaging

We next investigated whether the buried-ligand micro- bubbles could be used for in vivo ultrasound molecular imaging. Following microbubble injection, the tumor area was treated with 10 volumetric applications of USRF and then imaged for targeted microbubbles using an image-silence-image sequence (Figure 3A). Silencing of the contrast signal was necessary to delineate adherent from free microbubbles and was accomplished by fragmenting the intact microbubbles with a short, high–mechanical index pulse. The signal from adherent microbubbles was separated from that of freely circulating microbubbles and tissue artifact by taking the difference in video intensity for each voxel before and after the silencing pulse. The contrast signal from targeted microbubbles was registered to the tumor anatomy by overlaying the bound-microbubble signal in green to the background grayscale

B-mode image (Figure 3B). This method produced conspicuous images of the targeted microbubbles throughout the tumor volume, with a clear increase in the extent of contrast for cRGD microbubbles exposed to USRF in comparison with controls. This is to our knowledge the first time that ultrasonography has been used to activate targeting specificity for in vivo molecular imaging. All imaging procedures were performed using a commercially available clinical ultrasound system.

The ultrasound images were analyzed using a relatively simple algorithm to determine the volumetrically averaged contrast signal intensity in the tumor (ACI). This was done by taking the AVI in units of decibels by summing the ultrasound contrast video intensity values for each voxel within the tumor volume and dividing that value by the total number of voxels within that volume. The ACI in units of decibels was then computed by subtracting the background AVI obtained prior to the targeted micro- bubble injection from the AVI produced by the molecular imaging scan. This method of analysis provided a direct comparison between the different imaging parameters but did not correct for nonlinearities inherent in the imaging system. Thus, the ACI provided a semiquantitative measure of tumor neovasculature, and a comparison of the ACI between the microbubble formulations and ultrasound pulse sequences provided an assessment in the relative imaging sensitivity.

We investigated the effect of the application of acoustic radiation force pulsing (USRF enhancement). The USRF enhancement is determined by taking the ratio of the contrast-to-tissue ratios for tumors with and without exposure to USRF for a given microbubble architecture. The USRF is therefore normalized by circulation persistence to give a measure of the stimulus responsiveness. Exposure to USRF more than doubled the ACI volume for cRGD microbubbles (Figure 4A). No such increase was observed for control cRAD microbubbles in the same animals. A comparison of the USRF enhancement between brush architectures showed a twofold increase for the buried ligand compared to the exposed ligand (Figure 4B).

Discussion and Conclusion

Application of USRF with buried-ligand microbubbles was used for ultrasound molecular imaging of tumor neovasculature in vivo. Our data show that the PEG brush had the necessary barrier properties to avoid competitive interactions between the ligand and plasma components en route to the tumor. Our data also show that the microbubble surface is sufficiently dynamic to achieve firm adhesion between the buried-ligand microbubbles and tumor endothelium, even after the USRF field was removed. By overcoming these barriers, the ultrasound imaging method was able to detect angiogenic tumor regions with high sensitivity. The methodology allowed on-demand spatiotemporal control over microbubble adhesion, providing enhanced specificity to the targeted tumor tissue. Molecular specificity for $\alpha_v\beta_3$ integrin was shown by comparing the molecular imaging contrast signal from microbubbles expressing the targeting ligand versus those expressing the scrambled peptide control, in the same tumors. Finally, the utility of the technique was shown through the use of a widely available clinical scanner.

This work paves the way for a new generation of ultrasound imaging systems that deliver finer target sensitivity and adaptive user control for increased safety and accuracy. Although these studies are encouraging, we note that the fibrosarcoma tumor model tested here is known to exhibit active angiogenesis over the tumor volume. This allowed quantification through volumetric averaging of the contrast signal to produce a sensitive and specific readout of tumor neovasculature. Clinical translation, however, would require further testing of the methodology in tumors ranging in size, shape, and tissue depth and exhibiting variable degrees of angiogenesis. Additionally, clinical translation will require additional studies to assess diagnosis of tumor physiology in large- animal models exhibiting genetically derived and spontaneous tumors. The in vivo demonstration of the technique here with the clinical scanner provides a strong rationale to pursue such studies.

Acknowledgments

Financial disclosure of authors: This work was funded by NIH R01 EB 009066 to MAB and PAD.

References

1. Weissleder R, Pittet MJ. Imaging in the era of molecular oncology. Nature. 2008; 452:580–589. [PubMed: 18385732]
2. Allison M. Is personalized medicine finally arriving? Nat Biotechnol. 2008; 26:509–517. [PubMed: 18464779]
3. Klibanov AL, Rasche PT, Hughes MS, et al. Detection of individual microbubbles of ultrasound contrast agents - imaging of free- floating and targeted bubbles. Invest Radiol. 2004; 39:187–195. [PubMed: 15076011]
4. Szebeni J. Complement activation-related pseudoallergy: a new class of drug-induced acute immune toxicity. Toxicology. 2005; 216:106–121. [PubMed: 16140450]
5. Borden MA, Sarantos MR, Stieger SM, et al. Ultrasound radiation force modulates ligand availability on targeted contrast agents. Mol Imaging. 2006; 5:139–147. [PubMed: 16954028]
6. Chen CC, Borden MA. Ligand conjugation to bimodal poly (ethylene glycol) brush layers on microbubbles. Langmuir. 2010; 26:13183–13194. [PubMed: 20695557]
7. Borden MA, Zhang H, Gillies RJ, et al. A stimulus-responsive contrast agent for ultrasound molecular imaging. Biomaterials. 2008; 29:597–606. [PubMed: 17977595]
8. Chen CC, Borden MA. The role of poly(ethylene glycol) brush architecture in complement activation on targeted microbubble surfaces. Biomaterials. 2011; 32:6579–6587. [PubMed: 21683439]
9. Chen CC, Sirsi SR, Homma S, Borden MA. Effect of surface architecture on in vivo ultrasound contrast persistence of targeted size-selected microbubbles. Ultrasound Med Biol. 2012; 38:492–503. [PubMed: 22305060]
10. Dayton PA, Morgan KE, Klibanov ALS, et al. A preliminary evaluation of the effects of primary and secondary radiation forces on acoustic contrast agents. IEEE Trans Ultrasonics Ferroelectr Freq Control. 1997; 44:1264–1277.
11. Dayton P, Klibanov A, Brandenburger G, Ferrara K. Acoustic radiation force in vivo: a mechanism to assist targeting of microbubbles. Ultrasound Med Biol. 1999; 25:1195–1201. [PubMed: 10576262]
12. Dayton PA, Allen JS, Ferrara KW. The magnitude of radiation force on ultrasound contrast agents. J Acoust Soc Am. 2002; 112:2183–2192. [PubMed: 12430830]
13. Ruoslahti E. RGD and other recognition sequences for integrins. Annu Rev Cell Dev Biol. 1996; 12:697–715. [PubMed: 8970741]
14. Jeppesen C, Wong JY, Kuhl TL, et al. Impact of polymer tether length on multiple ligand-receptor bond formation. Science. 2001; 293:465–468. [PubMed: 11463908]

15. Feshitan JA, Chen CC, Kwan JJ, Borden MA. Microbubble size isolation by differential centrifugation. J Colloid Interface Sci. 2009; 329:316–324. [PubMed: 18950786]
16. Sirsi SR, Flexman ML, Vlachos F, et al. Contrast ultrasound imaging for identification of early responder tumor models to anti- angiogenic therapy. Ultrasound Med Biol. 2012; 38:1019–1029. [PubMed: 22425376]
17. Chen, CC. Engineering microbubbles with the buried-ligand architecture for targeted ultrasound molecular imaging [PhD dissertation]. New York: Columbia University; 2011.
18. Witthaut R, Farhood A, Smith CW, Jaeschke H. Complement and tumor-necrosis-factor-alpha contribute to MAC-1 (CD11B/CD18) up-regulation and systemic neutrophil activation during endotoxemia in vivo. J Leukocyte Biol. 1994; 55:105–111. [PubMed: 8283134]
19. Jun HY, Park SH, Kim HS, Yoon KH. Long residence time of ultrasound microbubbles targeted to integrin in murine tumor model. Acad Radiol. 2010; 17:54–60. [PubMed: 19815430]
20. Garrigues HJ, Rubinchikova YE, DiPersio CM, Rose TM. Integrin alpha(V)beta(3) binds to the RGD motif of glycoprotein B of Kaposi's sarcoma-associated herpesvirus and functions as an RGD- dependent entry receptor. J Virol. 2008; 82:1570–1580. [PubMed: 18045938]
21. Stieger SM, Dayton PA, Borden MA, et al. Imaging of angiogenesis using cadence contrast pulse sequencing and targeted contrast agents. Contrast Media Mol Imaging. 2008; 3:9–18. [PubMed: 18335479]
22. Feingold S, Gessner R, Guracar IM, Dayton PA. Quantitative volumetric perfusion mapping of the microvasculature using contrast ultrasound. Invest Radiol. 2010; 45:669–674. [PubMed: 20808232]
23. Gessner RC, Streeter JE, Kothadia R, et al. An in vivo validation of the application of acoustic radiation force to enhance the diagnostic utility of molecular imaging using 3-D ultrasound. Ultrasound Med Biol. 2012; 38:651–660. [PubMed: 22341052]
24. Schneider M. Characteristics of SonoVue (TM). Echocardiogr J Card. 1999; 16:743–746.
25. Streeter JE, Dayton PA. An in vivo evaluation of the effect of repeated administration and clearance of targeted contrast agents on molecular imaging signal enhancement. Theranostics. 2012; 3:93–98. [PubMed: 23424189]
26. Johnson K, Cianciolo R, Gessner RC, Dayton PA. A pilot study to assess markers of rental damage to the rodent kidney after exposure to 7 MHz ultrasound pulse sequences designed to cause microbubble translation and disruption. Ultrasound Med Biol. 2012; 38:168–172. [PubMed: 22104535]
27. Janssen BJ, Huizinga EG, Raaijmakers HC, et al. Structures of complement component C3 provide insights into the function and evolution of immunity. Nature. 2005; 437:505–511. [PubMed: 16177781]

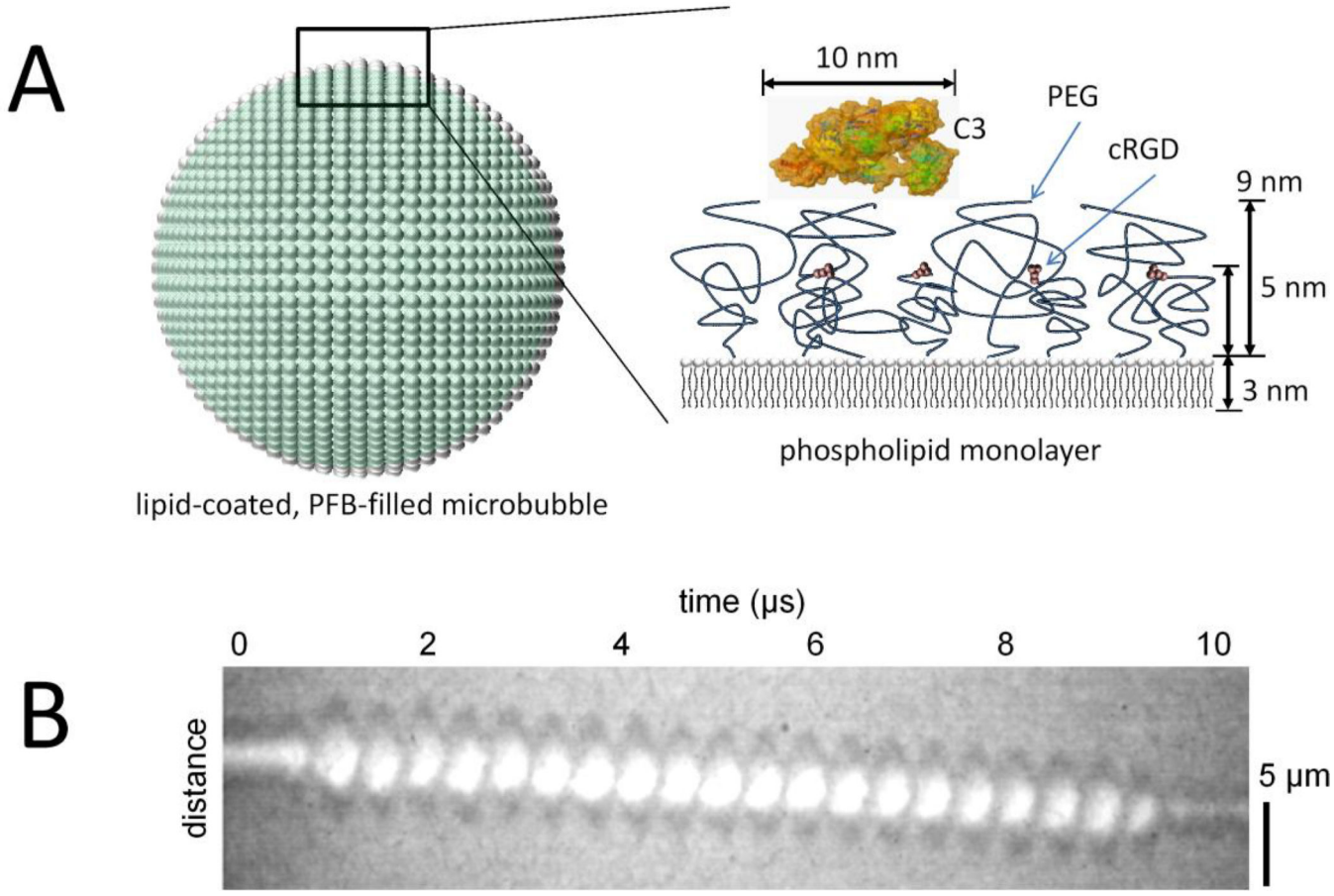

Figure 1.

Buried-ligand microbubbles and ultrasound radiation force. A, The ultrasound contrast agent is a microbubble of 4 to 5 μm diameter filled with perfluorobutane (PFB) gas and coated with a phospholipid monolayer shell. A side view of the shell shows the buried-ligand architecture, which comprises a shorter (2,000 Da) polyethylene glycol (PEG) tethered to cyclo Arg-Gly-Asp (cRGD) peptide surrounded by a longer (5,000 Da) PEG overbrush.[5–9] Also shown is a surface rendering of complement C3 protein.[27] B, A high- speed videomicroscopic streak image of the diameter of a microbubble over time shows acoustic radiation force acting on a microbubble to displace it axially away from the ultrasound transducer superimposed with surface dilations. These surface dilations expose the cRGD for binding to the target $\alpha_V\beta_3$ integrin.

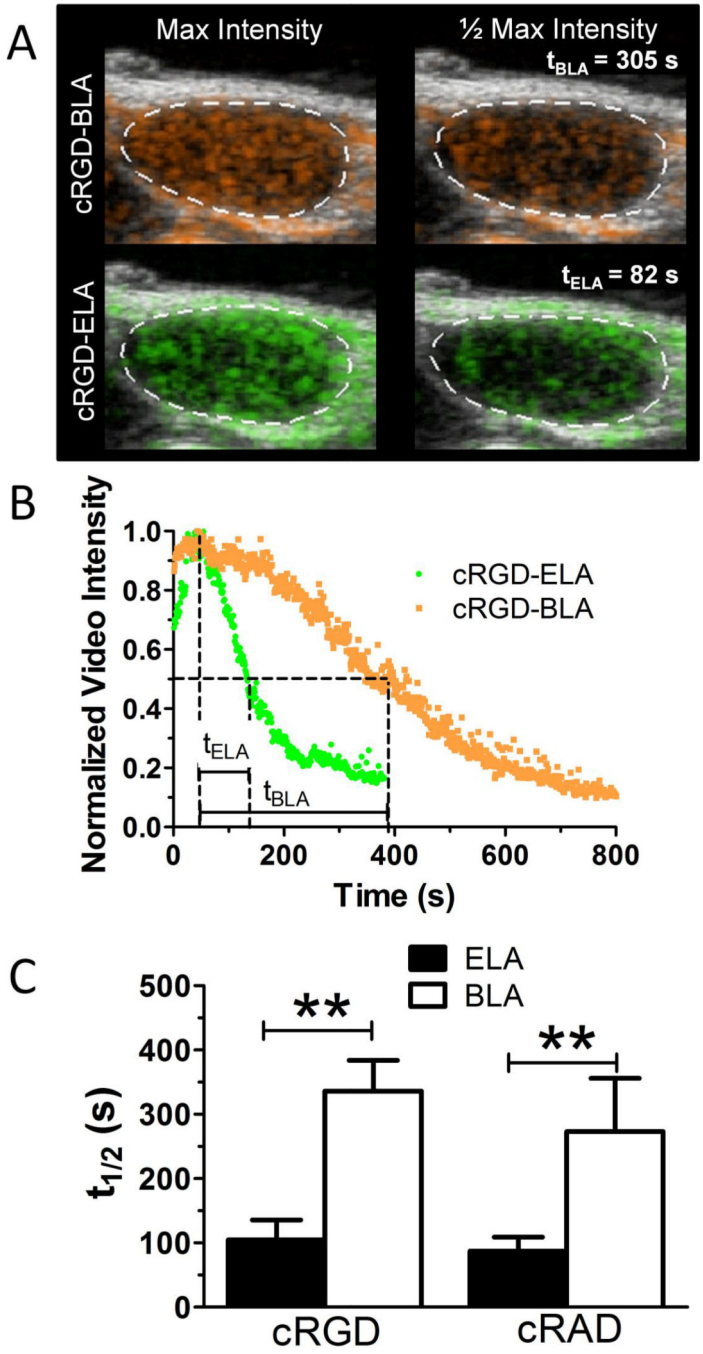

Figure 2.

Microbubble circulation persistence. A, Representative ultrasound images showing a two-dimensional image plane with color contrast from microbubble signals overlay onto grayscale B-mode images. B, Representative normalized time-intensity curves showing maximum and half-amplitudes. C, Analysis of total ultrasound contrast persistence in the tumor volume without ultrasound radiation force showed that buried-ligand microbubbles circulated approximately threefold longer than exposed-ligand microbubbles (cyclo Arg-Gly-Asp [cRGD], $p < .001$, $n \geq 5$; cyclo Arg-Ala- Asp [cRAD], $p < .001$, $n \geq 5$), indicating

avoidance of the mononuclear phagocyte system by the buried-ligand architecture (BLA). ELA 5 exposed- ligand architecture.

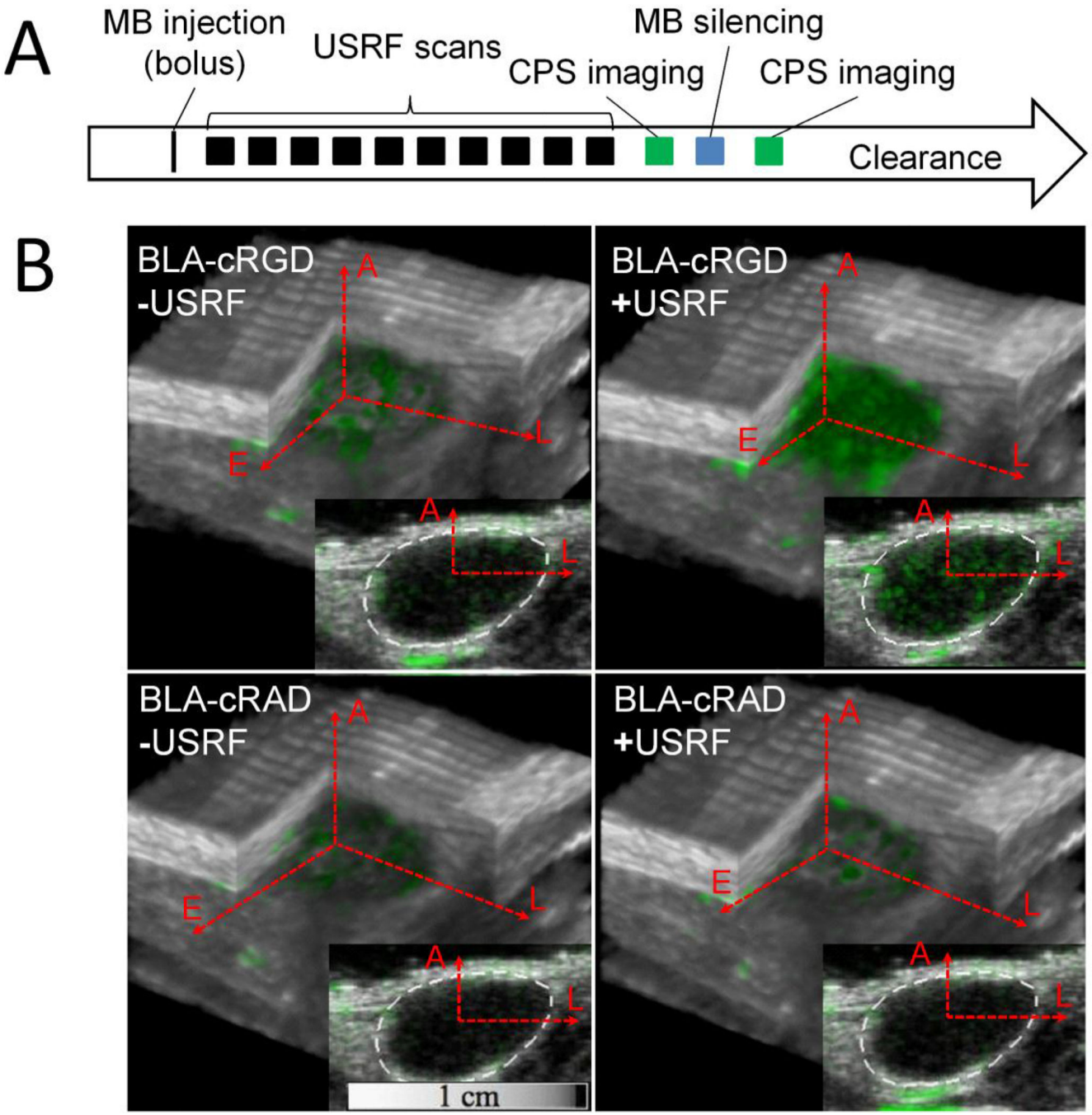

Figure 3.

In vivo ultrasound molecular imaging using buried-ligand microbubbles (MB) and ultrasound radiation force (USRF). A, The timeline for the rat xenograft fibrosarcoma experiments involved a single microbubble bolus tail-vein injection, followed by 10 USRF sweeps over the entire tumor volume, followed by an image-silence- image sequence to distinguish the signal from adherent microbubbles. Comparison of cyclo Arg-Gly-Asp (cRGD) with control scramble peptide cyclo Arg-Ala-Asp (cRAD)-conjugated microbubbles allowed determination of specificity. B, Images show the extent of buried-

ligand microbubble binding (green contrast) within the tumor and surrounding tissue. BLA = buried-ligand architecture; CPS = cadence pulse sequencing.

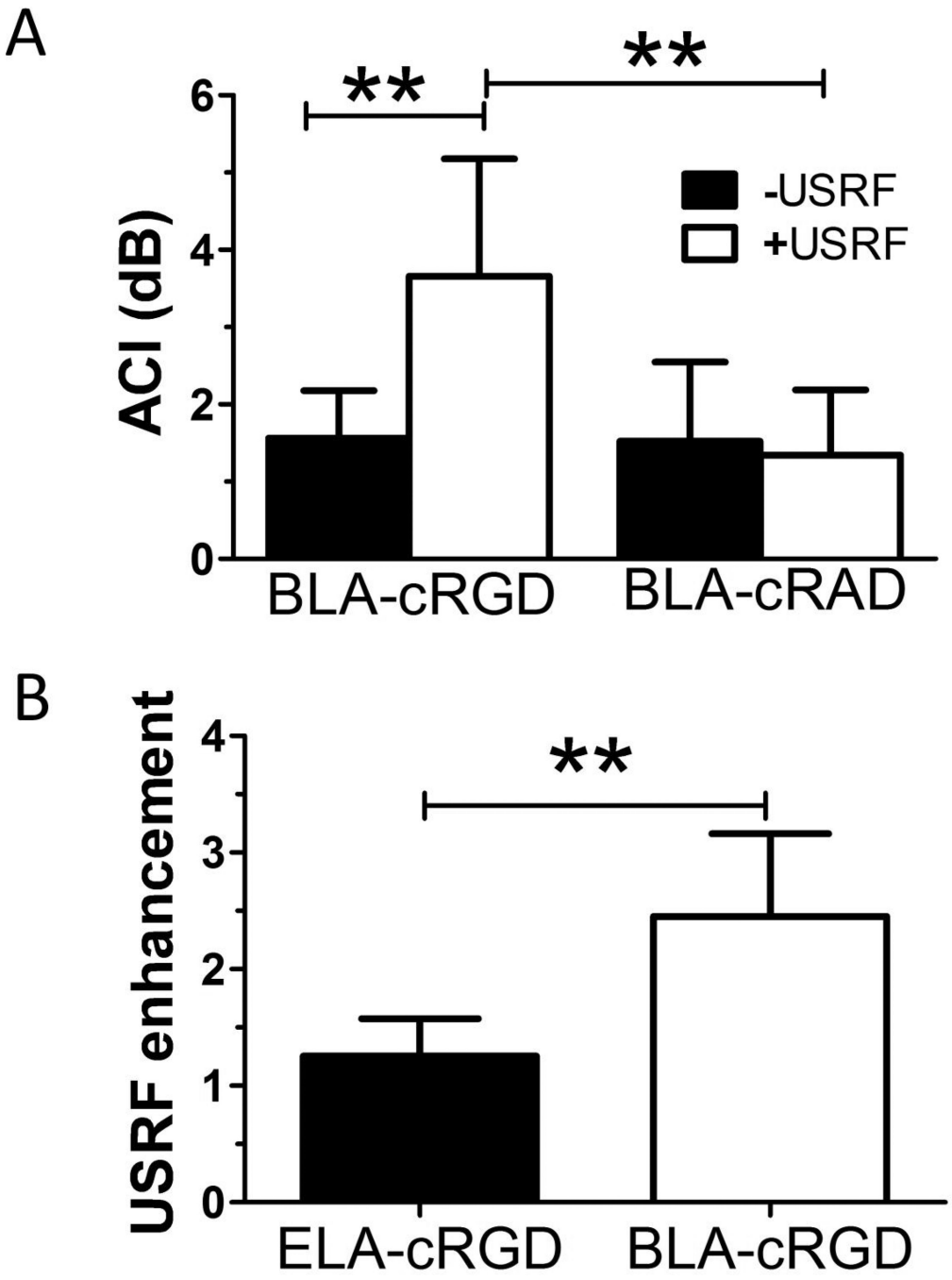

Figure 4.

Quantification of ultrasound molecular imaging. A, Analysis of the volumetric average contrast intensity (ACI) indicated a significant increase in cyclo Arg-Gly-Asp (cRGD) microbubble adhesion to neovasculature when exposed to ultrasound radiation force (USRF), showing that ultrasonography was effective in triggering ligand receptor–mediated adhesion ($n \geq 7$). Control cyclo Arg-Ala-Asp (cRAD) microbubbles experienced significantly less adhesion than cRGD microbubbles when stimulated with USRF, showing specificity ($n \geq 5$). B, Analysis of USRF enhancement for exposed-ligand architecture

(ELA) versus buried-ligand architecture (BLA) ($n \geq 7$). Enhancement was significantly greater for the BLA, showing that these microbubbles provide enhanced specificity to spatiotemporal targeting through application of radiation force. **$p < .01$.